Affine Frequency Division Multiplexing for Next-Generation Wireless Networks

Ali Bemani*, Giampaolo Cuozzo†, Nassar Ksairi‡, and Marios Kountouris*

*Communication Systems Department, EURECOM, Sophia Antipolis, France {ali.bemani, marios.kountouris}@eurecom.fr
†DEI, University of Bologna & Wilab, CNIT, giampaolo.cuozzo@unibo.it
‡Mathematical and Algorithmic Sciences Lab, Huawei France R&D, Paris, France, nassar.ksairi@huawei.com

Abstract—**Affine Frequency Division Multiplexing (AFDM) is a new multi-chirp waveform that can be generated and demodulated using the discrete affine Fourier transform (DAFT). DAFT is a generalization of discrete Fourier transform characterized with two parameters which can be adapted to better cope with both doubly dispersive channels and impairments at high-frequency bands. DAFT domain impulse response can indeed convey a full delay-Doppler representation of linear time-varying (LTV) channels, which allows AFDM to achieve the full diversity. Moreover, AFDM signals are maximally spread in time and frequency, thus providing a coverage gain that turns out to be robust against radio frequency impairments, such as carrier frequency offset and phase noise. In this paper, we show that AFDM offers the aforementioned advantages while being compatible with practical pilot-aided channel estimation and low-complexity channel equalization. Our analytical and simulation results evince that AFDM achieves significant throughput and reliability gains over state-of-the-art multicarrier modulation.**

Index Terms—**AFDM, affine Fourier transform, chirp modulation, linear time-varying channels, doubly dispersive channels, extremely high frequency bands.**

I. INTRODUCTION

Next-generation wireless systems (e.g., beyond 5G/6G) are envisioned to support a wide range of services including communication in high mobility scenarios and in extremely high-frequency (EHF) bands. This calls for new waveform design able to cope with various highly demanding requirements. Existing waveforms, orthogonal frequency division multiplexing (OFDM) in particular, have proved to achieve satisfactory or even optimal performance in time-invariant frequency selective channels. Nevertheless, this ceases to be true in high-mobility scenarios, double dispersive channels, and high-frequency bands. OFDM does not achieve full diversity in linear time-varying (LTV) channels [1]. Impairments that become significant at high frequencies, such as carrier frequency offset (CFO) and phase noise (PN) [2], could destroy orthogonality among OFDM subcarriers deteriorating performance. Moreover, high-frequency wireless links may suffer from severe pathloss, thus requiring waveforms with inherent coverage enhancement capabilities (not offered by OFDM or single-carrier waveforms).

Chirp-based modulation is a promising alternative for communication in time-varying channels. Finding an orthonormal basis decomposition for general LTV channels is not trivial. Employing an orthonormal basis formed by chirps (i.e., complex exponentials with linearly varying instantaneous frequencies) - despite not being optimal - can be adjusted to the channel characteristics as a means to achieve near-optimal performance. Using a chirp basis based on fractional Fourier transform (FrFT) instead of the sine basis for transmission over LTV channels is first introduced in [3]. A multicarrier technique based on discrete affine Fourier transform (DAFT), referred to as DAFT-OFDM in the sequel, is proposed in [4]. Its parameters are properly tuned using partial channel state information (CSI), namely the delay-Doppler profile of the channel (known delays and the Doppler shifts of channel paths), to reduce the inter-carrier interference (ICI). While this property is useful for supporting low-complexity detection, being equivalent to OFDM implies a diversity order close to that of OFDM (which is known to be low without channel coding). In addition, to tune the DAFT-OFDM parameters, the delay-Doppler profile of the channel is required at the transmitter side. Orthogonal chirp division multiplexing (OCDM) [5] uses a discrete Fresnel transform, which can be obtained as a special case of DAFT, and outperforms OFDM on time-dispersive channels thanks to a higher diversity order. Orthogonal time frequency space (OTFS) modulation [1] is a two-dimensional (2D) modulation technique that uses the delay-Doppler domain for multiplexing information. OTFS can achieve the full diversity of LTV channels provided the data constellation is rotated in a specific manner [6] and achieves full *effective* diversity order, i.e., the diversity order in the finite signal-to-noise ratio (SNR) regime as defined in [7]. However, it comes with several drawbacks in terms of pilot overhead and multiuser multiplexing overhead [8] due to the 2D nature of the underlying transform. Other chirp-based waveforms, such as chirp spread spectrum (CSS) [9], have been proposed for power-limited wireless links and could be relevant for many high-frequency scenarios. Indeed, CSS signals are maximally spread in time and frequency, offering a coverage gain i.e., the possibility of increasing the signal-to-noise ratio (SNR) at the receiver through spreading in time, thus doing away with inefficient SNR enhancement schemes such as symbol repetition. However, CSS achievable rates are limited due to the non-orthogonality of its multiplexed chirps.

Affine frequency division multiplexing (AFDM) is a recently proposed waveform [10] that employs multiple orthogonal information-bearing chirps generated using the inverse DAFT (IDAFT). In this paper, after a brief overview of
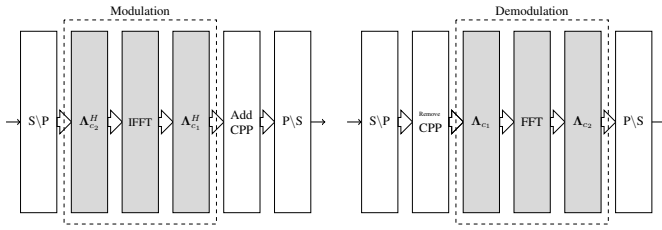
Fig. 1. AFDM modulation/demodulation block diagram

AFDM, we analyze its performance in two scenarios: high-mobility and high-frequency bands. In the former, AFDM is shown to provide a full delay-Doppler representation of the doubly dispersive channel, which allows to achieve full diversity. Moreover, we propose a low-overhead pilot-aided channel estimation scheme and a low-complexity linear minimum mean square error (LMMSE) detector. In EHF bands, AFDM is shown to be maximally spread in time and frequency, thus providing a coverage gain. While maximal time-frequency spreading can be offered by other waveforms (e.g., OTFS, CSS), AFDM is distinguished by the fact that the benefits of maximal spreading are achieved while detection is (i) performed using one-tap equalization and (ii) robust to CFO and phase noise.

The paper is organized as follows. AFDM is introduced in Section II. Section III shows the optimality of AFDM in terms of diversity gain in high-mobility scenarios. The potential of AFDM for high-frequency scenarios is established in Section IV. Simulation results are provided in Section V, while Section VI concludes the paper.

II. AFFINE FREQUENCY DIVISION MULTIPLEXING

A. Modulation and Demodulation

DAFT, which is the basis of AFDM, is a discretized version of the AFT [10]–[13]. Let $\mathbf{x}$ denote a vector of N quadrature amplitude modulation (QAM) symbols. As shown in Fig. 1, inverse DAFT (IDAFT) is used to map $\mathbf{x}$ to the time domain

$$s_n = \frac{1}{\sqrt{N}} \sum_{m=0}^{N-1} x_m e^{\imath 2\pi(c_2 m^2 + \frac{1}{N}mn + c_1 n^2)}, \quad n = 0, \cdots, N-1. \tag{1}$$

In matrix form, (1) becomes

$$\mathbf{s} = \mathbf{\Lambda}_{c_1}^H \mathbf{F}^H \mathbf{\Lambda}_{c_2}^H \mathbf{x}. \tag{2}$$

where $\mathbf{F}$ is the discrete Fourier transform (DFT) matrix with entries $e^{-\imath 2\pi mn/N}/\sqrt{N}$ and $\mathbf{\Lambda}_c = \mathrm{diag}(e^{-\imath 2\pi cn^2}, n = 0, 1, \ldots, N-1)$. Like OFDM, AFDM needs a prefix to make the channel seemingly lie in a periodic domain. However, this prefix should be a *chirp-periodic* prefix (CPP) defined as

$$s_n = s_{N+n} e^{-\imath 2\pi c_1(N^2 + 2Nn)}, \quad n = -L, \cdots, -1. \tag{3}$$

Here, L is any integer greater than or equal to the value in samples of the maximum delay spread of the wireless channel. Note that a CPP is simply a CP whenever $2Nc_1$ is integer and

N is even. After parallel to serial conversion and transmission over the channel, the received samples as

$$r_n = \sum_{l=0}^{\infty} s_{n-l} g_n(l) + w_n, \tag{4}$$

where $w_n \sim \mathcal{CN}(0, N_0)$ is additive Gaussian noise and $g_n(l)$ is the impulse response of channel at time n and delay l. The DAFT domain output symbols are obtained by

$$y_m = \frac{1}{N} \sum_{n=0}^{N-1} r_n e^{-\imath 2\pi(c_2 m^2 + \frac{1}{N}mn + c_2 n^2)}. \tag{5}$$

After discarding the CPP, the output can be written in matrix representation as

$$\mathbf{y} = \mathbf{\Lambda}_{c_2} \mathbf{F} \mathbf{\Lambda}_{c_1} \mathbf{r} = \mathbf{H}_{\mathrm{eff}} \mathbf{x} + \widetilde{\mathbf{w}} \tag{6}$$

where $\mathbf{H}_{\mathrm{eff}} = \mathbf{\Lambda}_{c_2} \mathbf{F} \mathbf{\Lambda}_{c_1} \mathbf{H} \mathbf{\Lambda}_{c_1}^H \mathbf{F}^H \mathbf{\Lambda}_{c_2}^H$, $\mathbf{H}$ is the matrix representation of the channel, $\widetilde{\mathbf{w}} = \mathbf{\Lambda}_{c_2} \mathbf{F} \mathbf{\Lambda}_{c_1} \mathbf{w}$ and $\mathbf{w} \sim \mathcal{CN}(\mathbf{0}, N_0 \mathbf{I})$. Since $\mathbf{\Lambda}_{c_2} \mathbf{F} \mathbf{\Lambda}_{c_1}$ is a unitary matrix, $\widetilde{\mathbf{w}}$ and $\mathbf{w}$ have the same covariance.

III. AFDM FOR HIGH MOBILITY COMMUNICATION

In this section we assume that the wireless channel is time-varying and has the following impulse response

$$g_n(l) = \sum_{i=1}^{P} h_i e^{-\imath 2\pi f_i n} \delta(l - l_i) \tag{7}$$

where $P \geq 1$ is the number of paths, $\delta(\cdot)$ is the Dirac delta function, and h_i, f_i and l_i are the complex gain, Doppler shift (in digital frequencies), and the integer delay associated with the i-th path, respectively. It should be noted that this model is general and covers the case where each delay tap can have a Doppler frequency spread by simply allowing for different paths $i, j \in \{1, \ldots, P\}$ to have the same delay $l_i = l_j$ while satisfying $f_i \neq f_j$. We define $\nu_i \triangleq N f_i = \alpha_i + a_i$, where $\nu_i \in [-\nu_{\max}, \nu_{\max}]$ is the Doppler shift normalized with respect to the subcarrier spacing, $\alpha_i \in [-\alpha_{\max}, \alpha_{\max}]$ is its integer part while a_i is the fractional part satisfying $\frac{-1}{2} < a_i \leq \frac{1}{2}$. For the sake of simplicity, we assume that the fractional parts a_i are zero. In addition, we assume that the maximum delay of the channel satisfies $l_{\max} \triangleq \max(l_i) < N$. The channel matrix is

$$\mathbf{H} = \sum_{i=1}^{P} h_i \mathbf{\Gamma}_{\mathrm{CPP}_i} \mathbf{\Delta}_{f_i} \mathbf{\Pi}^{l_i} \tag{8}$$

where $\mathbf{\Pi}$ is the forward cyclic-shift matrix, $\mathbf{\Delta}_{f_i} \triangleq \mathrm{diag}(e^{-\imath 2\pi f_i n}, n = 0, 1, \ldots, N-1)$ and

$$\mathbf{\Gamma}_{\mathrm{CPP}_i} \triangleq$$

$$\mathrm{diag}(\begin{cases} e^{-\imath 2\pi c_1(N^2 - 2N(l_i - n))} & n < l_i \\ 1 & n \geq l_i \end{cases}, n = 0, \ldots, N-1).$$
$$\tag{9}$$

Defining $\mathbf{H}_i \triangleq \mathbf{\Lambda}_{c_2} \mathbf{F} \mathbf{\Lambda}_{c_1} \mathbf{\Gamma}_{\mathrm{CPP}_i} \mathbf{\Delta}_{f_i} \mathbf{\Pi}^{l_i} \mathbf{\Lambda}_{c_1}^H \mathbf{F}^H \mathbf{\Lambda}_{c_2}^H$, (6) can be rewritten as

$$\mathbf{y} = \sum_{i=1}^{P} h_i \mathbf{H}_i \mathbf{x} + \tilde{\mathbf{w}}. \tag{10}$$
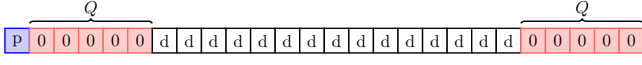
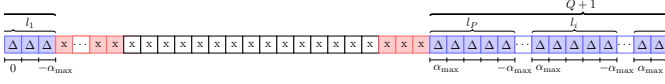Fig. 2. AFDM symbol pattern ('P': pilot, 'd': data, '0': guard)

Fig. 3. Received DAFT domain samples ('Δ': pilot samples, 'x: data')

It is shown in [10] that if c_1 is chosen such that $2Nc_1$ is an integer, the entry in row p and column q of $\mathbf{H}_i$ writes as

$$[\mathbf{H}_i]_{p,q} = \begin{cases} e^{i\frac{2\pi}{N}(Nc_1l_i^2 - ql_i + Nc_2(q^2-p^2))} & q = (p+\text{loc}_i)_N \\ 0 & \text{otherwise} \end{cases},$$
(11)

where $\text{loc}_i \triangleq \alpha_i + 2Nc_1l_i$. Hence, there is only one non-zero element in each row of $\mathbf{H}_i$ and its location in the p-th row is $(p+\text{loc}_i)_N$. The input-output relation in (10) becomes

$$y_p = \sum_{i=1}^{P} h_i e^{i\frac{2\pi}{N}(Nc_1l_i^2 - ql_i + Nc_2(q^2-p^2))} x_q + \tilde{w}, 0 \le p \le N-1$$
(12)

where $q = (p+\text{loc}_i)_N$. Parameters c_1 and c_2 can be set in a way that the DAFT domain impulse response constitutes a full delay-Doppler representation of the channel. For that sake, the unique non-zero entry in each row of $\mathbf{H}_i$ for each path $i \in \{1, \ldots, P\}$ should not coincide with the position of the unique non-zero entry of the same row of $\mathbf{H}_j$ for any $j \in \{1, \ldots, P\} \setminus \{i\}$. It is shown in [10] that by setting

$$c_1 = \frac{2\alpha_{\max} + 1}{2N}.$$
(13)

and assuming N is large enough so that $2\alpha_{\max}l_{\max} + 2\alpha_{\max} + l_{\max} < N$, channel paths with different delay values or different Doppler frequency shifts get separated in the DAFT domain, resulting in $\mathbf{H}_{\text{eff}}$ having the delay-Doppler representation of the channel in the DAFT domain. With c_1 satisfying (13) and c_2 set to be an arbitrary irrational number or a rational number sufficiently smaller than $\frac{1}{2N}$, AFDM achieves the full diversity of the LTV channels [10].

A. Embedded pilot transmission and channel estimation

Channel estimation can be performed by inserting in the AFDM frame $\mathbf{x}$ one pilot symbol, x_{pilot}, surrounded by L_g guard symbols with $N-1-L_g$ data symbols occupying the rest of the frame. To perform channel estimation and data detection without data/pilot interference, the number of guard symbols should satisfy $L_g \ge 2Q$ where $Q \triangleq 2l_{\max}\alpha_{\max} + 2\alpha_{\max} + l_{\max}$. Fig. 2 shows an AFDM frame with x_{pilot} occupying the first entry of $\mathbf{x}$. At the receiver, the samples $y_p, 0 \le p \le \alpha_{\max}, N_Q + \alpha_{\max} + 1 \le p \le N-1$ where $N_Q = N-(Q+1)$ are the entries of $\mathbf{y}$ relevant for channel estimation as can be seen from Fig. 3. Referring to (12), these samples are given

by

$$y_p = \begin{cases} h_i' x_{\text{pilot}} + w_p, & \exists i \in \{1, \ldots, P\}, p = (N-\text{loc}_i)_N, \\ w_p, & \text{otherwise} \end{cases}.$$
(14)

Here, $h_i' \triangleq h_i e^{i\frac{2\pi}{N}(Nc_1l_i^2 - Nc_2p^2)}$. As can be seen from (14), the entries y_p which are not pure noise are used for the channel estimation. The delay-Doppler profile of the channel can be estimated from their locations p and the complex gains are estimated using the value of these entries as they are the complex gains scaling x_{pilot}.

B. Data detection

To recover the transmitted data symbols, we apply channel equalization to the entries of the demodulated samples vector $\mathbf{y}$ occupied by data-related samples (marked as 'x' in Fig. 3). Let $\underline{\mathbf{y}} \triangleq \mathbf{T}_r\mathbf{y}$ be the truncated version of $\mathbf{y}$ corresponding to these entries where $\mathbf{T}_r \triangleq [\mathbf{I}_N]_{\alpha_{\max}+1:N_Q+\alpha_{\max},:}$. Then

$$\underline{\mathbf{y}} = \underline{\mathbf{H}}_{\text{eff}}\underline{\mathbf{x}} + \underline{\tilde{\mathbf{w}}},$$
(15)

where $\underline{\mathbf{x}} \triangleq \mathbf{T}_t\mathbf{x}$, $\mathbf{T}_t \triangleq [\mathbf{I}_N]_{Q+1:N_Q+1,:}$ and $\underline{\mathbf{H}}_{\text{eff}} \triangleq \mathbf{T}_r\mathbf{H}_{\text{eff}}\mathbf{T}_t^H$. Referring to (15), the LMMSE estimate of $\underline{\mathbf{x}}$ is

$$\hat{\underline{\mathbf{x}}} = \underline{\mathbf{H}}_{\text{eff}}^H(\underline{\mathbf{H}}_{\text{eff}}\underline{\mathbf{H}}_{\text{eff}}^H + N_0\mathbf{I}_{N_Q})^{-1}\underline{\mathbf{y}}.$$
(16)

Matrix $\mathbf{M} \triangleq \underline{\mathbf{H}}_{\text{eff}}\underline{\mathbf{H}}_{\text{eff}}^H + N_0\mathbf{I}_{N_Q}$ is a Hermitian band matrix with lower and upper bandwidth Q. This structure can be exploited to compute $\mathbf{M}^{-1}$ using, say, the LDL^H decomposition. It can be shown that instead of cubic order complexity, computing $\hat{\underline{\mathbf{x}}}$ using such a decomposition only needs $(2Q^2 + 11Q + 4)N_Q$ complex operations.

IV. AFDM FOR HIGH FREQUENCY BANDS

We now turn our attention to communication at high frequency bands without mobility. Wireless transmissions in these bands suffer from impairments such as carrier frequency offset (CFO), phase noise (PN) and severe pathloss (PL) [2], [14]. In this section, we configure AFDM by setting c_1 to $\frac{1}{2N}$ (a value that can be obtained by plugging $\alpha_{\max} = 0$ into (13)). The relevance for high-frequency scenarios of setting c_1 to different values will be addressed in future works. We next show that AFDM with this configuration can provide a coverage gain that is robust under CFO and PN and which is compatible with one-tap equalization. This remarkable property is thanks to the way AFDM with $c_1 = c_2 = \frac{1}{2N}$ becomes a waveform with both single-carrier and multi-carrier features, as shown in the following subsection. Without loss of generality, we only consider receiver side CFO and PN.

A. AFDM input-output relation under CFO and PN

In the remainder of this section, we reuse the notation $\mathbf{H}_{\text{eff}}$ originally introduced in (6) to make it refer to the effective DAFT domain channel matrix in presence of the considered impairments. We then introduce the new notation $\mathbf{H}_{\text{eff,free}}$ ("free" as in free from impairments) to designate the DAFT domain channel matrix when transmission undergoes no such impairments. Note by referring to (11) that $\mathbf{H}_{\text{eff,free}}$

is circulant for the no-mobility scenario considered here. Let $\mathbf{P}$ be a diagonal matrix having as its main diagonal entries the multiplicative time domain complex exponentials resulting from a receiver side CFO equal (when normalized with respect to the subcarrier spacing) to ν_{CFO} and the N time domain receiver side PN samples $\{\varphi_n\}_{n=0\ldots N-1}$

$$[\mathbf{P}]_{n,n} = e^{\imath 2\pi \frac{\nu_{\text{CFO}}}{N} n} e^{\imath 2\pi \varphi_n}. \tag{17}$$

The effective channel matrix in presence of receiver side CFO and PN thus writes as

$$\begin{aligned} \mathbf{H}_{\text{eff}} &= \boldsymbol{\Lambda}_{c_2} \mathbf{F} \boldsymbol{\Lambda}_{c_1} \mathbf{P} \boldsymbol{\Lambda}_{c_1}^{\text{H}} \mathbf{F}^H \boldsymbol{\Lambda}_{c_2}^{\text{H}} \mathbf{H}_{\text{eff,free}} \\ &= \boldsymbol{\Lambda}_{c_2} \mathbf{F} \mathbf{P} \mathbf{F}^H \boldsymbol{\Lambda}_{c_2}^{\text{H}} \mathbf{H}_{\text{eff,free}}, \end{aligned} \tag{18}$$

where the second equality is due to the fact that $\boldsymbol{\Lambda}_{c_1}$ is diagonal. Note that in the case with no impairments, $\mathbf{P} = \mathbf{I}_N$ and $\mathbf{H}_{\text{eff}} = \mathbf{H}_{\text{eff,free}}$. In the general case, the absolute value of $\boldsymbol{\Lambda}_{c_2} \mathbf{F} \mathbf{P} \mathbf{F}^H \boldsymbol{\Lambda}_{c_2}^{\text{H}}$ is circulant because $\boldsymbol{\Lambda}_{c_2}$ is diagonal. To get better insight into the input-output relation of AFDM as conveyed by (18) we first consider two scenarios in both of which the transmission undergoes only one impairment: only CFO in the first and only PN in the second.

Only-CFO scenario: It is reasonable to assume that $\nu_{\text{CFO}} < 1$ since in practice at least rough frequency synchronization is implemented. Under this assumption and $\varphi_n = 0$ for all n in (17), it can be shown that the absolute value of the q-th entry ($q \in \{0,\ldots,N-1\}$) of the first row of matrix $\boldsymbol{\Lambda}_{c_2} \mathbf{F} \mathbf{P} \mathbf{F}^H \boldsymbol{\Lambda}_{c_2}^{\text{H}}$ is $\left| \frac{\sin \pi (q - \nu_{\text{CFO}})}{\sin \frac{\pi}{N} (q - \nu_{\text{CFO}})} \right|$. Since this matrix is circulant in absolute value, it follows that the power of the entries of its diagonals decreases the farther they are from the main diagonal. Moreover, due to the quadratic phase of the entries of $\boldsymbol{\Lambda}_{c_2}$, the phase of the entries of each diagonal of the matrix $\boldsymbol{\Lambda}_{c_2} \mathbf{F} \mathbf{P} \mathbf{F}^H \boldsymbol{\Lambda}_{c_2}^{\text{H}}$ is affine in the column (or row) index with a frequency equal when normalized with respect to the subcarrier spacing to the index of the diagonal (with the main diagonal having the zero index). More precisely, the k-th entry of $\mathbf{y} = \mathbf{H}_{\text{eff}} \mathbf{x}$ ($k \in \{0,\ldots,N-1\}$) is

$$y_k = \sum_{i=1}^{P} \sum_{q=0}^{N-1} h_i e^{\imath \left(\phi_{i,q} + 2\pi \frac{qk}{N}\right)} \frac{\sin \pi (q - \nu_{\text{CFO}})}{\sin \frac{\pi}{N} (q - \nu_{\text{CFO}})} x_{(k+l_i+q)_N}, \tag{19}$$

where $\phi_{i,q}$ only depends on l_i, q and N. Due to the decay profile of $\left| \frac{\sin \pi(q-\nu_{\text{CFO}})}{\sin \frac{\pi}{N}(q-\nu_{\text{CFO}})} \right|$ as function of q, the root mean square (RMS) of the frequency shifts q expressed in Hz i.e., $\frac{1}{NT_s} \sqrt{\sum_{q=0}^{N-1} q^2 \frac{\sin^2 \pi(q-\nu_{\text{CFO}})}{\sin^2 \frac{\pi}{N}(q-\nu_{\text{CFO}})} / \sum_{q=0}^{N-1} \frac{\sin^2 \pi(q-\nu_{\text{CFO}})}{\sin^2 \frac{\pi}{N}(q-\nu_{\text{CFO}})}}$, where T_s is the sampling period, can be shown to be 1) increasing with ν_{CFO} and 2) approximately constant in N.

Only-PN scenario: Assuming the PN is modeled as a first-order auto-regressive AR(1) process and $\nu_{\text{CFO}} = 0$ in (17), it can be shown as in [15, Appendix A] that the entries of the diagonals of the circulant matrix $\mathbf{F} \mathbf{P} \mathbf{F}^H$ (and hence those of the matrix $\boldsymbol{\Lambda}_{c_2} \mathbf{F} \mathbf{P} \mathbf{F}^H \boldsymbol{\Lambda}_{c_2}^{\text{H}}$ which is circulant in absolute value) have mean powers averaged over the PN process realizations that decay the farther the diagonal is from the main diagonal [15]. As in the CFO scenario, the phase evolution of the

entries of each diagonal of $\boldsymbol{\Lambda}_{c_2} \mathbf{F} \mathbf{P} \mathbf{F}^H \boldsymbol{\Lambda}_{c_2}^{\text{H}}$ has a frequency equal when normalized with respect to the subcarrier spacing to the index of the diagonal. Also, the RMS of these frequency shifts in Hz can be shown to be increasing with the RMS of the AR(1)-PN process and approximately independent of N.

Both-CFO-and-PN scenario: Combining the two scenarios and referring to (18), the effect of both CFO and phase noise on the DAFT domain channel response can be verified to be cumulative and amounting to mapping each diagonal in $\mathbf{H}_{\text{eff,free}}$ representing a channel path to a "spectrum" of frequency shifted and attenuated diagonals in $\mathbf{H}_{\text{eff}}$, possibly partially overlapping with the spectra corresponding to other channel paths, and whose effective width increases with the CFO value and the RMS of the PN process while being approximately constant in N when normalized by it.

Result 1. *The input-output relation of AFDM in presence of CFO and AR(1)-PN is that of an equivalent time domain channel subject to a Doppler spread whose RMS is increasing with the CFO value and with the RMS of the PN process and approximately constant in N when expressed in Hz.*

B. AFDM robust spreading gain

By *robustness* in presence of impairments we mean relative advantage to other waveforms in terms of relevant performance metrics e.g., bit error rate (BER), when channel estimation and data detection are done without knowing the values of these impairments e.g., the CFO in Hz or the time domain phase noise samples in radians. In the case of OFDM, impairment-agnostic detection amounts to ignoring ICI and using one-tap equalization based on (an estimate of) the main diagonal of the frequency domain channel matrix[1]. In the case of AFDM with $c_1 = c_2 = \frac{1}{2N}$, an impairment-agnostic receiver would do channel estimation and equalization assuming the DAFT domain channel matrix $\mathbf{H}_{\text{eff}}$ to be circulant (while it is only circulant in the absence of the impairments as can be seen from (18)). One possible detection method when $\mathbf{H}_{\text{eff}}$ is assumed circulant is one-tap equalization applied using an estimate of the main diagonal of the DFT factorization of this matrix. Consider a N-point AFDM frame $\mathbf{x} = \mathbf{A}_{\text{u}} \mathbf{x}_{\text{u}}$ composed of $N_{\text{u}} > 1$ ('u' for "used") data symbols represented by vector $\mathbf{x}_{\text{u}}$ and occupying contiguous positions within $\mathbf{x}$ with $N_{\text{u}} \leq N$. Here, $\mathbf{A}_{\text{u}}$ is the $N \times N_{\text{u}}$ matrix that maps the non-zero data symbols to their positions. Let

$$\mathbf{y} = \mathbf{H}_{\text{eff}} \mathbf{A}_{\text{u}} \mathbf{x}_{\text{u}} + \mathbf{w} \tag{20}$$

be the N-long vector of received DAFT domain samples (after AFDM demodulation). Note that $\mathbf{H}_{\text{eff}} \mathbf{A}_{\text{u}}$ is not a square matrix and hence not circulant even in the absence of impairments. The effective channel matrix associated with $\mathbf{x}_{\text{u}}$ can though be made square (and circulant in the absence

---

[1]The estimate of the main diagonal of the channel matrix of an OFDM symbol in presence of these impairments can be obtained either based on pilots embedded in the same symbol or based on pilots embedded in previous symbols. Note that common phase error (CPE) estimation and compensation is needed in the latter case but not in the former.

of impairments) by applying overlap-add (OLA) [16] to the entries of $\mathbf{y}$ corresponding to the $N - N_{\mathrm{u}}$ zero samples of $\mathbf{x}$. Let $\mathbf{y}_{\mathrm{u}} \triangleq \mathbf{A}_{\mathrm{OLA}}\mathbf{y}$ be the resulting vector with $\mathbf{A}_{\mathrm{OLA}}$ being the $N_{\mathrm{u}} \times N$ matrix representing the OLA operation. Then

$$\mathbf{y}_{\mathrm{u}} = \mathbf{H}_{\mathrm{eff},\mathrm{u}}\mathbf{x}_{\mathrm{u}} + \mathbf{A}_{\mathrm{OLA}}\mathbf{w}, \qquad (21)$$

where

$$\mathbf{H}_{\mathrm{eff},\mathrm{u}} \triangleq \mathbf{A}_{\mathrm{OLA}}\mathbf{H}_{\mathrm{eff}}\mathbf{A}_{\mathrm{u}}. \qquad (22)$$

It follows that the one-tap LMMSE estimate of $\mathbf{x}_{\mathrm{u}}$ is

$$\hat{\mathbf{x}}_{\mathrm{u}} = \mathrm{IDFT}\left\{\left(\mathrm{diag}\left(\tilde{\mathbf{H}}_{\mathrm{eff},\mathrm{u}}\right)^{\mathrm{H}}\mathrm{diag}\left(\tilde{\mathbf{H}}_{\mathrm{eff},\mathrm{u}}\right) + \mathbf{\Sigma}_{\mathbf{w}}\right)^{-1}\tilde{\mathbf{y}}_{\mathrm{u}}\right\} \qquad (23)$$

where $\tilde{\mathbf{y}}_{\mathrm{u}} \triangleq \mathrm{DFT}\{\mathbf{y}_{\mathrm{u}}\}$, $\tilde{\mathbf{H}}_{\mathrm{eff},\mathrm{u}} \triangleq \mathbf{F}_{N_{\mathrm{u}}}\mathbf{H}_{\mathrm{eff},\mathrm{u}}\mathbf{F}_{N_{\mathrm{u}}}^{\mathrm{H}}$ and $\mathbf{\Sigma}_{\mathbf{w}}$ is the $N_{\mathrm{u}} \times N_{\mathrm{u}}$ (diagonal) covariance matrix of the noise samples vector $\mathbf{A}_{\mathrm{OLA}}\mathbf{w}$. Of course, when the transmission is subject to CFO or PN, $\mathbf{H}_{\mathrm{eff}}$ as given by (18) and $\mathbf{H}_{\mathrm{eff},\mathrm{u}}$ as given by (22) are not circulant. As a result, $\tilde{\mathbf{H}}_{\mathrm{eff},\mathrm{u}}$ is not diagonal. The main diagonal of $\tilde{\mathbf{H}}_{\mathrm{eff},\mathrm{u}}$ can still be estimated based on one embedded pilot symbol as in subsection III-A but the performance of the one-tap equalizer in (23) based on this estimate suffers from ICI due to the off-diagonal entries of $\tilde{\mathbf{H}}_{\mathrm{eff},\mathrm{u}}$. However, due to the property summarized by Result 1, this degradation will be of the order of what would be undergone by an equivalent N_{u}-point (and not N-point) OFDM transmission with N_{u} active subcarriers taking place on the same wireless channel in presence of the same impairments. It will then have the higher robustness of the larger subcarrier spacing $\frac{1}{N_{\mathrm{u}}} \geq \frac{1}{N}$.

Now, refer to (1) and note that a constraint on the time domain transmit power such as $\mathbb{E}\left[|s_n|^2\right] \leq P_{\mathrm{tx}}$ translates into $\mathbb{E}\left[|x_m|^2\right] \leq \frac{N}{N_{\mathrm{u}}}P_{\mathrm{tx}}$. This means that increasing N at a constant N_{u} and P_{tx} provides a $\frac{N}{N_{\mathrm{u}}}$-times increase in the effective SNR associated with detecting $\hat{\mathbf{x}}_{\mathrm{u}}$ in (23). Combining this fact with the higher-robustness property described above shows that for small-enough values of N_{u} compared to N, this SNR increase translates into an increase in the signal-to-interference-plus-noise ratio (SINR).

Result 2. *The one-tap equalization in* (23) *for a N-point AFDM signal with $N_{\mathrm{u}} \leq N$ active data symbols and a transmit power equal to P_{tx} has under CFO and AR(1)-PN the SINR performance of an equivalent N_{u}-point OFDM with a $\frac{N}{N_{\mathrm{u}}}P_{\mathrm{tx}}$ transmit power under a Doppler spread with a RMS proportional to the CFO and the PN RMS values.*

One application of this result is coverage enhancement in power-limited scenarios that are also subject to CFO and PN e.g., mmWave, sub-THz and THz communications under severe pathloss [2], [14] and/or imperfect antenna beam alignment between the wireless transmitter and receiver.

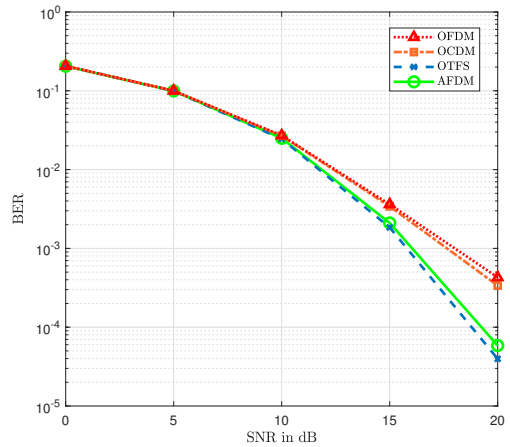**Remark 1.** *In multiple-access settings, the robust spreading gain offered by AFDM does not come at the cost of*

Fig. 4. BER performance of OCDM, and AFDM with $N = 256$ and OTFS with $N_{\mathrm{OTFS}} = 16$ and $M_{\mathrm{OTFS}} = 16$ using QPSK and LMMSE detection assuming a 21-path LTV channel with $l_{\max} = 2$ and $\alpha_{\max} = 3$

reduced system spectral efficiency. Indeed, while each multiplexed spread AFDM signal occupies the frequency bandwidth and time duration of the whole multicarrier symbol, different spread AFDM signals occupy orthogonal resources in the DAFT domain. This is in contrast to coverage gain enhancement using symbol repetition for single-carrier (SC) waveforms with time-division multiple access (TDMA).

V. SIMULATION RESULTS

We first compare the BER performance of AFDM to that of OFDM, OCDM [5] and OTFS [1] in a high-mobility scenario. Fig. 4 which is obtained using 10^6 different channel realizations with complex gains h_i generated as independent complex Gaussian random variables with zero mean and $1/P$ variance shows the performance of OFDM, OCDM, AFDM with $N = 256$ and OTFS with $N_{\mathrm{OTFS}} = 16$ and $M_{\mathrm{OTFS}} = 16$, using QPSK symbols and LMMSE detection in a 21-path LTV channel with $l_{\max} = 2$ and $\alpha_{\max} = 3$. For each delay tap, there are 7 paths with different Doppler shifts from -3 to 3. It can be seen that due to the destructive addition of overlapping paths, OFDM and OCDM exhibit the worst performance. Moreover, AFDM and OTFS have the same performance in terms of BER. However, OTFS needs a pilot overhead twice that of AFDM due to the 2D structure of its underlying transform. Indeed, while the embedded pilot scheme presented in subsection III-A occupies $2\left(2\alpha_{\max} + 1\right)\left(l_{\max} + 1\right) - 1$ entries out of the N entries of the AFDM symbol, its OTFS counterpart [8] requires $\left(4\alpha_{\max} + 1\right)\left(2l_{\max} + 1\right)$. This difference translates in an advantage of AFDM over OTFS in terms of spectral efficiency as shown in Fig. 5. The spectral efficiency values were derived from the BER values plotted in Fig. 4.

We now compare the BER performance of AFDM and OFDM, both using one-tap equalization receivers, in a high-frequency scenario characterized with a low transmit power, large pathloss, severe phase noise and no CFO. Fig. 6 was obtained assuming a line-of-sight (LoS) channel with $P = 1$, a zero Doppler shift $f_1 = 0$, a delay l_1 that is derived from
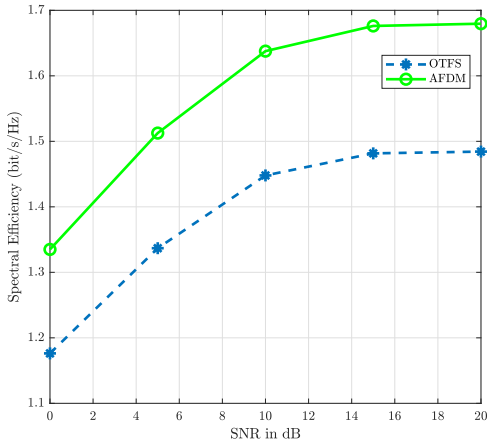
Fig. 5. Spectral efficiency performance of AFDM with $N = 256$ and OTFS with $N_{\mathrm{OTFS}} = 16$ and $M_{\mathrm{OTFS}} = 16$ using QPSK and LMMSE detection assuming a 21-path LTV channel with $l_{\max} = 2$ and $\alpha_{\max} = 3$
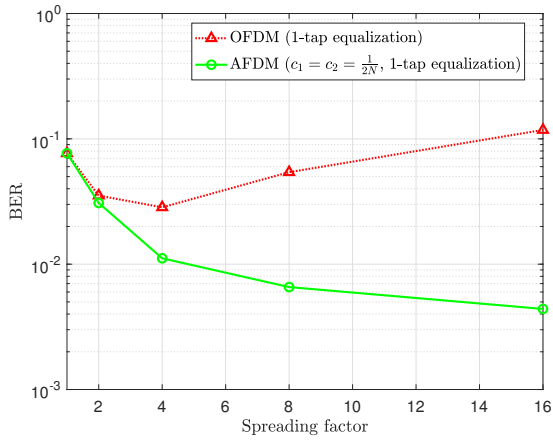

Fig. 6. BER performance of OFDM and AFDM with using QPSK with $N_{\mathrm{u}} = 64$, $N =$ spreading factor$\times N_{\mathrm{u}}$ assuming a LoS THz channel with $d = 1$ m, $f_{\mathrm{c}} = 0.35$ THz, BW $= 0.5$ GHz, $B_{3-\mathrm{dB}}^{\mathrm{PN}} = 60$ kHz, $P_{\mathrm{tx}} = -3$ dBm and $G_{\mathrm{Tx}} = G_{\mathrm{Rx}} = 27$ dBi

the distance d separating the transmitter from the receiver. The variance of the complex gain h_1 was computed using the THz pathloss model from [14] assuming a carrier frequency $f_{\mathrm{c}} = 0.35$ THz and 27-dBi antenna gains. The receiver side phase noise was generated using a AR(1) random process having a power spectral density with a 3-dB bandwidth $B_{3-\mathrm{dB}}^{\mathrm{PN}}$ of approximately 60 kHz. This value was obtained starting from a typical value of $B_{3-\mathrm{dB}}^{\mathrm{PN}}$ for an oscillator operating at 2.4 GHz [17] and then scaled to account for the higher carrier frequency using the scaling laws from [17], [18]. The number of data symbols per OFDM and AFDM frame is $N_{\mathrm{u}} = 64$ and the transmit power is equal to $P_{\mathrm{tx}} = -3$ dBm for both schemes. When $N = N_u$, the SNR and the SINR associated with one-tap equalization are both low for both OFDM and AFDM resulting in a relatively large BER. Increasing N while keeping N_{u} and P_{tx} fixed increases the received SNR for both schemes. For AFDM, this translates into an increase in SINR and a decrease in BER thanks to its robust spreading/coverage gain property. As for OFDM, increasing N inversely reduces the subcarrier spacing resulting in degraded BER performance.

VI. Conclusions

In this paper, we presented AFDM, a new waveform based on multiple discrete-time orthogonal chirp signals, and showed its relevance for communication in both high mobility and high frequency scenarios. AFDM is shown to achieve the full diversity of linear time-varying channels. Additionally, it provides a spreading gain that is robust to carrier frequency offsets and phase noise. These advantages and its throughput and reliability performance keeping the complexity low render AFDM eminently promising for next-generation wireless systems.

References

[1] R. Hadani, S. Rakib, M. Tsatsanis, A. Monk, A. J. Goldsmith, A. F. Molisch, and R. Calderbank, "Orthogonal time frequency space modulation," in *2017 IEEE Wireless Communications and Networking Conference (WCNC)*. IEEE, 2017, pp. 1–6.

[2] H. Huang, W. G. J. Wang, and J. He, "Phase noise and frequency offset compensation in high frequency MIMO-OFDM system," in *2015 IEEE International Conference on Communications (ICC)*, 2015, pp. 1280–1285.

[3] M. Martone, "A multicarrier system based on the fractional Fourier transform for time-frequency-selective channels," *IEEE Trans. on Commun.*, vol. 49, no. 6, pp. 1011–1020, Jun. 2001.

[4] T. Erseghe, N. Laurenti, and V. Cellini, "A multicarrier architecture based upon the affine Fourier transform," *IEEE Trans. on Commun.*, vol. 53, no. 5, pp. 853–862, May 2005.

[5] X. Ouyang and J. Zhao, "Orthogonal chirp division multiplexing," *IEEE Trans. on Commun.*, vol. 64, no. 9, pp. 3946–3957, Sept. 2016.

[6] G. Surabhi, R. M. Augustine, and A. Chockalingam, "On the diversity of uncoded OTFS modulation in doubly-dispersive channels," *IEEE Trans. on Wireless Communications*, vol. 18, no. 6, pp. 3049–3063, 2019.

[7] P. Raviteja, Y. Hong, E. Viterbo, and E. Biglieri, "Effective diversity of OTFS modulation," *IEEE Wireless Communications Letters*, Feb. 2019.

[8] P. Raviteja, K. T. Phan, and Y. Hong, "Embedded pilot-aided channel estimation for OTFS in delay–doppler channels," *IEEE Trans. on Vehicular Technology*, vol. 68, no. 5, pp. 4906–4917, 2019.

[9] B. Reynders and S. Pollin, "Chirp spread spectrum as a modulation technique for long range communication," in *2016 Symposium on Communications and Vehicular Technologies (SCVT)*, 2016, pp. 1–5.

[10] A. Bemani, N. Ksairi, and M. Kountouris, "AFDM: A full diversity next generation waveform for high mobility communications," in *2021 IEEE International Conference on Communications Workshops (ICC Workshops)*, 2021, pp. 1–6.

[11] M. Moshinsky and C. Quesne, "Linear canonical transformations and their unitary representations," *Journal of Mathematical Physics*, vol. 12, no. 8, pp. 1772–1780, Aug. 1971.

[12] S.-C. Pei and J.-J. Ding, "Relations between fractional operations and time-frequency distributions, and their applications," *IEEE Trans. on Sig. Proc.*, vol. 49, no. 8, pp. 1638–1655, Aug. 2001.

[13] S. Pei and J. Ding, "Closed-form discrete fractional and affine Fourier transforms," *IEEE Trans. on Sig. Proc.*, vol. 48, no. 5, pp. 1338–1353, May 2000.

[14] E. N. Papasotiriou, J. Kokkoniemi, A.-A. A. Boulogeorgos, J. Lehtomäki, A. Alexiou, and M. Juntti, "A new look to 275 to 400 GHz band: Channel model and performance evaluation," in *2018 IEEE 29th Annual International Symposium on Personal, Indoor and Mobile Radio Communications (PIMRC)*, 2018, pp. 1–5.

[15] G. Sridharan and T. J. Lim, "Performance analysis of sc-fdma in the presence of receiver phase noise," *IEEE Transactions on Communications*, vol. 60, no. 12, pp. 3876–3885, 2012.

[16] S. Salivahanan and A. Vallavaraj, *Digital Signal Processing*. McGraw-Hill, 2001.

[17] C. M. Yuen and K. F. Tsang, "Phase noise measurement of free-running vco using spectrum analyzer," in *Proceedings. 2004 IEEE Radio and Wireless Conference (IEEE Cat. No.04TH8746)*, 2004, pp. 443–446.

[18] D. Petrovic, W. Rave, and G. Fettweis, "Effects of phase noise on ofdm systems with and without pll: Characterization and compensation," *IEEE Transactions on Communications*, vol. 55, no. 8, pp. 1607–1616, 2007.